

Predicting the ground-state structure of sodium boride

Xin-Ling He,¹ Xiao Dong,¹ QuanSheng Wu,² Zhisheng Zhao,³ Qiang Zhu,⁴ Artem R. Oganov,^{5,6,7} Yongjun Tian,³ Dongli Yu,³ Xiang-Feng Zhou,^{1,*} and Hui-Tian Wang^{1,8}

¹Key Laboratory of Weak-Light Nonlinear Photonics, School of Physics, Nankai University, Tianjin 300071, China

²Institute of Physics, National Centre for Computational Design and Discovery of Novel Materials MARVEL, École Polytechnique Fédérale de Lausanne (EPFL), CH-1015 Lausanne, Switzerland

³State Key Laboratory of Metastable Materials Science and Technology, Yanshan University, Qinhuangdao 066004, China

⁴Department of Physics and Astronomy, High Pressure Science and Engineering Center, University of Nevada, Las Vegas, Nevada 89154, USA

⁵Skolkovo Institute of Science and Technology, 3 Nobel Street, Moscow 143026, Russia

⁶Moscow Institute of Physics and Technology, Dolgoprudny, Moscow Region 141700, Russia

⁷International Center for Materials Discovery, Northwestern Polytechnical University, Xi'an 710072, China

⁸National Laboratory of Solid State Microstructures, Collaborative Innovation Center of Advanced Microstructures, Nanjing University, Nanjing 210093, China



(Received 2 October 2017; revised manuscript received 5 March 2018; published 26 March 2018)

Binary borides has been a subject of extensive research. However, the exact compositions and crystal structures of sodium borides remained controversial. Here, using the *ab initio* variable-composition evolutionary algorithm, a new stable Na₂B₃₀ with $I2_12_12_1$ symmetry ($I2_12_12_1$ -Na₂B₃₀) is found, which is -7.38 meV/atom lower in energy than the *Imma*-Na₂B₃₀ structure reported by experimentalists. Interestingly, the *Imma*-Na₂B₃₀ structure is predicted to be a topological nodal line semimetal, which may result in superior electronic transport. In contrast, $I2_12_12_1$ -Na₂B₃₀ is an ultrahard semiconductor with an unprecedented open-framework structure, whose interstitial helical boron sublattice enhances its hardness and energetic stability.

DOI: [10.1103/PhysRevB.97.100102](https://doi.org/10.1103/PhysRevB.97.100102)

The discovery of high-temperature superconductivity, superhardness, ferromagnetism, and quantum topological properties in metal borides has attracted much attention owing to many interesting fundamental issues and huge potential applications [1–6]. For alkali-metal borides, only a few compounds have been precisely determined with regard to their compositions and structures. This is mainly limited by the synthesis and characterization of these materials, e.g., it is difficult to conduct a controlled reaction between the low-melting alkali metals with boron under ambient pressure, and their products are often microcrystalline powders rather than single crystals [7–10]. So far, there are only two sodium borides, orthorhombic Na₃B₂₀ and Na₂B₃₀ (or monoclinic Na₂B₂₉), which were successfully synthesized at ambient pressure [7–9]. However, the exact structure and composition of “*Imma*-Na₂B₃₀” are still controversial. Previously, Naslain and Kasper refined the structure as orthorhombic Na₂B₃₀ (designated as the ϕ phase) [7]. This structure consists principally of B₁₂ icosahedra with interstitial boron triangular units, with Na atoms accommodated in the cages formed by icosahedra [7]. Since the unit cell of Na₂B₃₀ contains four formula units, it could be written as 4(NaB₃B₁₂). However, by using x-ray diffraction (XRD), neutron diffraction, electron microscopy, and solid-state NMR spectroscopy, Albert *et al.* revised the structure as monoclinic Na₂B₂₉ (2(NaB₃B₁₂ + NaB₂B₁₂)) with two interstitial B atoms per unit cell unoccupied (*Cm*-Na₂B₂₉) [8]. To study the controversy, we performed *ab initio* calculations for the two

structural models and found that: (1) the relaxed Na₂B₂₉ had orthorhombic symmetry (*Imm2*-Na₂B₂₉), which is inconsistent with the reported monoclinic symmetry [8]; (2) *Imma*-Na₂B₃₀ is energetically more favorable than *Imm2*-Na₂B₂₉ in the Na-B system; (3) the band structure shows that *Imma*-Na₂B₃₀ is a topological nodal line semimetal rather than a metal [11]. These intriguing results inspire us to further explore the polymorphism, phase diagram, and properties of this important compound.

To find stable Na-B compounds and structures, we utilized the *ab initio* evolutionary algorithm USPEX [12], performing searches with up to 40 atoms per primitive cell and searching for all stable stoichiometries and their corresponding structures simultaneously. A phase is deemed stable if its enthalpy of formation from either elements or any other possible compounds is negative, and such a method has been successfully applied to various bulk systems [13–16]. Structure relaxations and total-energy calculations used the all-electron projector-augmented wave [17] method as implemented in the VASP package [18] with [1s²] cores for both Na and B atoms, the exchange-correlation energy was treated within the generalized gradient approximation (GGA) using the functional of Perdew, Burke, and Ernzerhof (PBE) [19]. In addition, the local density approximation (LDA) with the functional of Ceperley and Alder [20] as parametrized by Perdew and Zunger [21] was also employed to confirm the energetic stability. The plane-wave cutoff energy of 500 eV and uniform Γ -centered k -point grids with a resolution of $2\pi \times 0.04 \text{ \AA}^{-1}$ were used. Denser k -point grids were tested but produced indistinguishable results. The convergence for terminating the electronic self-consistent

*xfzhou@nankai.edu.cn; zxf888@163.com

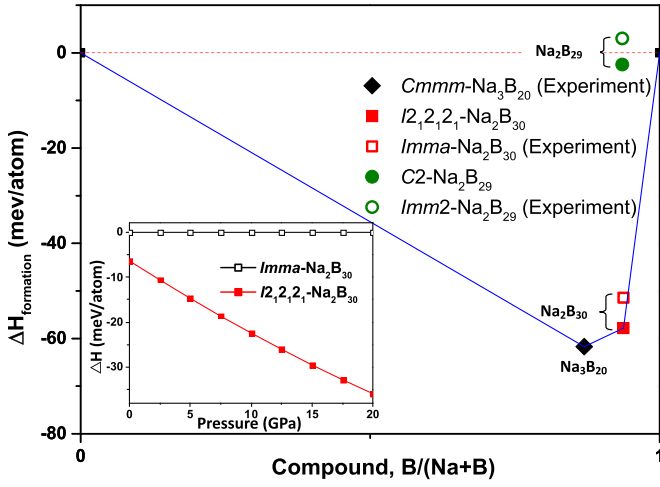


FIG. 1. The calculated convex hull for the Na-B system, using *bcc*-Na and α -boron structures for pure elements. Here, $\Delta H_{\text{formation}}(\text{Na}_x\text{B}_{1-x}) = H(\text{Na}_x\text{B}_{1-x}) - xH(\text{Na}) - (1-x)H(\text{B})$. The inset shows the enthalpy difference between *Imma*- Na_2B_{30} and *I212121*- Na_2B_{30} as a function of pressure.

cycle and the force criterion for structure relaxation were set at 10^{-6} eV and 10^{-2} eV/Å, respectively. Phonon dispersion curves were calculated using the finite displacement method as implemented in the PHONOPY package [22] where the convergence criterion for the total energy was 10^{-6} eV. Elastic tensors were computed via stress-strain relations. Combined with the Voigt-Reuss-Hill approximation [23], the bulk and shear moduli were calculated by the CASTEP code at the GGA-PBE level [24]. Powder XRD patterns were simulated using the REFLEX software [24]. Topological properties were investigated by constructing maximally localized Wannier functions [25] using the WANNIERTOOLS code [26].

The convex hull plotted in Fig. 1 showed two stable compounds at ambient pressure, Na_3B_{20} and Na_2B_{30} , consistent with the available experimental reports. Especially, the predicted lattice constants and atomic positions for Na_3B_{20} are in excellent agreement with the experimental values [9]. This illustrates the power, reliability, and accuracy of the USPEX method. However, the experimental *Imm2*- Na_2B_{29} structure has a positive formation energy (3.03 meV/atom) and is far from the convex hull. Additionally, the structure search also found a new monoclinic Na_2B_{29} (*C2*- Na_2B_{29}), which had lower formation energy (-2.45 meV/atom) than *Imm2*- Na_2B_{29} but still above the convex hull formed by Na_3B_{20} and Na_2B_{30} , indicating that both structures of Na_2B_{29} are at best metastable phases. Unexpectedly, it was not the much-discussed *Imma*- Na_2B_{30} but a new polymorph *I212121*- Na_2B_{30} that appeared on the convex hull and therefore predicted to be one of the true ground-state phases in the Na-B system because it has lower enthalpy than the mixture of elemental Na and B or any other mixtures. As shown in Table I, the GGA-PBE results show that *I212121*- Na_2B_{30} is -6.37 and -60.84 meV/atom lower in formation energy than the *Imma*- Na_2B_{30} and *Imm2*- Na_2B_{29} structures. The LDA calculations show the corresponding values are -18.14 and -77.34 meV/atom accordingly, i.e., both the GGA-PBE and

TABLE I. Lattice constants, energy of formation (ΔE_f with units of meV/atom), density (ρ), shear modulus (G), bulk modulus (B), and the calculated Vickers hardness (H_v) of sodium borides. Some experimental values (from Refs. [7,8]) are also listed for comparison.

Parameters	Na_2B_{30}	Na_2B_{30}	Na_2B_{29}	Experiments
<i>Symmetry</i>	<i>I212121</i>	<i>Imma</i>	<i>Imm2</i>	<i>Cm</i> ⁸ , <i>Imma</i> ⁷
<i>a</i> (Å)	10.42	10.29	10.34	10.40 ⁸ , 10.30 ⁷
<i>b</i> (Å)	5.70	5.84	5.82	5.86 ⁸ , 5.85 ⁷
<i>c</i> (Å)	8.23	8.42	8.31	8.33 ⁸ , 8.42 ⁷
ΔE_f (GGA)	-57.81	-51.44	3.03	N/A
ΔE_f (LDA)	-63.37	-45.23	13.97	N/A
ρ (g/cm ⁻³)	2.52	2.43	2.39	2.34 ⁸ , 2.44 ⁷
<i>G</i> (GPa)	189.02	162.50	142.03	N/A
<i>B</i> (GPa)	190.05	179.32	167.22	N/A
<i>H_v</i> (GPa)	37.40	30.23	25.53	N/A

the LDA give the same ranking of structures by stability. Inclusion of zero-point energy from the GGA-PBE results only strengthens our conclusion: *I212121*- Na_2B_{30} is now more stable than *Imma*- Na_2B_{30} by -7.38 meV/atom. Moreover, the enthalpy difference (as a function of pressure; see the inset of Fig. 1) confirms that *I212121*- Na_2B_{30} is more stable than *Imma*- Na_2B_{30} at any pressure.

These two crystal structures are compared in Fig. 2. For the *Imma*- Na_2B_{30} structure, the Na atom sits at Na (0.000,0.250,0.089), six inequivalent B sites are B1 (0.202, 0.089,0.915), B2 (0.169,0.002,0.713), B3 (0.395,0.250,0.144), B4 (0.649,0.250,0.903), B5 (0.000,0.250,0.497), and B6 (0.915,0.250,0.796). Among them, Na, B3, and B5 are interstitial atoms, i.e., not belonging to any B_{12} icosahedra. The icosahedra are connected either by direct intericosahedral B-B bonds (two-electron-two-center bonds with the lengths of 1.766 and 1.755 Å) or by three-center bonds with bond lengths of 2.078 and 1.746 Å [see Figs. 2(a) and 2(b)]. The *Imm2*- Na_2B_{29} structure, as mentioned above, is just a modified version of *Imma*- Na_2B_{30} , obtained by removing two interstitial B atoms from their interstitial triangular boron units in the unit cell, resulting in a 3.33% boron vacancy concentration. On the other hand, atomic positions in the *I212121*- Na_2B_{30} structure are completely different from those of *Imma*- Na_2B_{30} [see Figs. 2(c) and 2(d)]: Na (0.000,0.250,0.149), eight inequivalent B atoms occupy sites B1 (0.587,0.741,0.363), B2 (0.332,0.996,0.039), B3 (0.171,0.478,0.953), B4 (0.191,0.095, 0.337), B5 (0.917,0.238,0.469), B6 (0.189,0.419,0.339), B7 (0.840,0.232,0.663), and B8 (0.368,0.000,0.250). Among them, the interstitial B1 and B8 atoms form a peculiar helical sublattice, linking B_{12} icosahedra by multicenter B-B-B bonds with varied bond lengths ranging from 1.711 to 2.058 Å.

Table I compares calculated properties of various models of Na_2B_{30} and Na_2B_{29} with experimental values. All three models have similar lattice constants and densities (compare lattice parameters of *I212121*- Na_2B_{30} with the experimental values [7,8], the maximum difference in lattice parameters *a*, *b*, and *c* are 1.16%, 2.56%, and 2.25%), and all three are in good agreement with experimental results. It is unsurprising that *Imma*- Na_2B_{30} and *Imm2*- Na_2B_{29} have similar lattice constants because they are just two versions of the

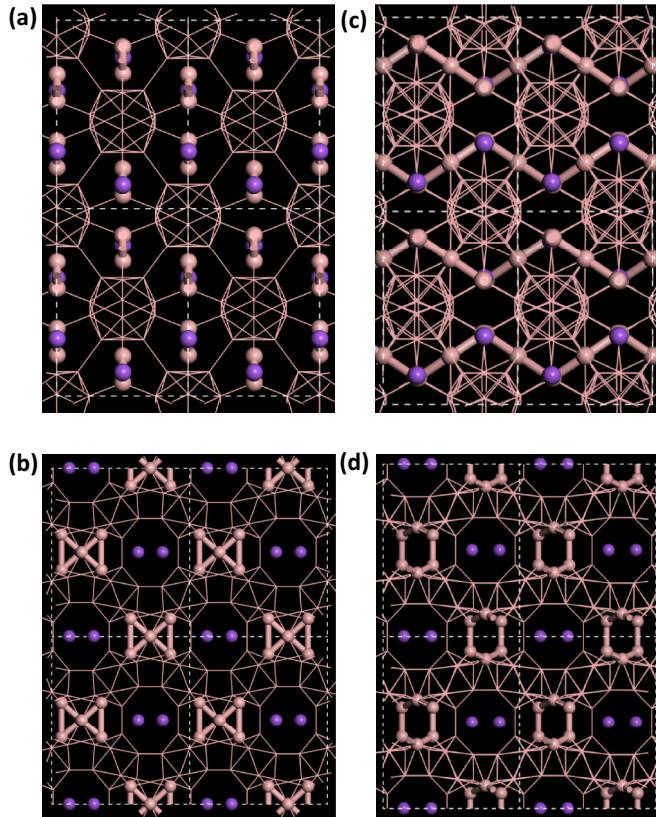


FIG. 2. Structures of $Imma\text{-Na}_2\text{B}_{30}$ and $I2_12_12_1\text{-Na}_2\text{B}_{30}$. (a) Projection of $Imma\text{-Na}_2\text{B}_{30}$ along the [100] direction. (b) Projection of $Imma\text{-Na}_2\text{B}_{30}$ along the [010] direction. (c) Projection of $I2_12_12_1\text{-Na}_2\text{B}_{30}$ along the [100] direction. (d) Projection of $I2_12_12_1\text{-Na}_2\text{B}_{30}$ along the [010] direction. The Na and B atoms are colored in purple and brown, and the interstitial B atoms in the two structures are magnified for clarity.

same structure, whereas $I2_12_12_1\text{-Na}_2\text{B}_{30}$ has a completely different structural topology. Therefore, we simulated the x-ray-diffraction patterns of the $Imm2\text{-Na}_2\text{B}_{29}$, $Imma\text{-Na}_2\text{B}_{30}$, and $I2_12_12_1\text{-Na}_2\text{B}_{30}$ structures and compared them with the experimental results [8]. As shown in Fig. 3(a), there is good agreement, both for the positions and the intensities of most peaks for all of the three models and experiments, including the (200), (211), (301), (220), (312), (213), (321), and (325) peaks. The other simulated peaks with 2θ from 45° to 70° are too weak to be used for quantitative analysis [8]. Note that the (101) peak is absent in $I2_12_12_1\text{-Na}_2\text{B}_{30}$ and the intensities of the (011) and (002) peaks deviate from experimental values to some extent. We speculate that $I2_12_12_1\text{-Na}_2\text{B}_{30}$ may coexist with $Imma\text{-Na}_2\text{B}_{30}$ (or Na_2B_{29}) at ambient conditions. Moreover, the comparison of the measured electron-diffraction pattern (TEM) along the [010] direction [Fig. 3(b)] showed that the diffraction spots of all three models again match well with the experimental data [8]. Since the $I2_12_12_1\text{-Na}_2\text{B}_{30}$ structure is very different from $Imma\text{-Na}_2\text{B}_{30}$ or $Imm2\text{-Na}_2\text{B}_{29}$, this example shows that very different structures can have very similar XRD and TEM patterns, making structure determination ambiguous, and in such cases the input from theory is invaluable.

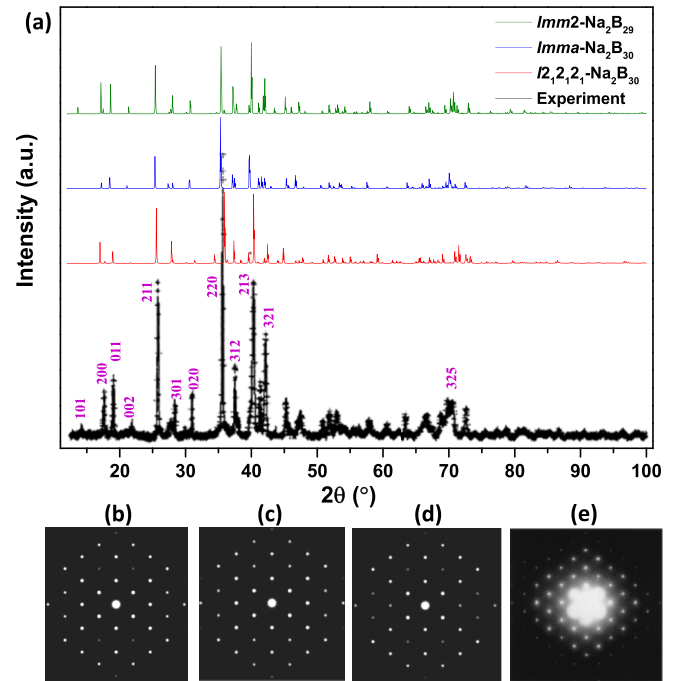


FIG. 3. (a) Simulated XRD patterns of $Imm2\text{-Na}_2\text{B}_{29}$, $Imma\text{-Na}_2\text{B}_{30}$, and $I2_12_12_1\text{-Na}_2\text{B}_{30}$ with a wavelength of 1.54056 \AA at ambient pressure compared with the experimental results. (b) Simulated TEM patterns of $Imm2\text{-Na}_2\text{B}_{29}$, (c) $Imma\text{-Na}_2\text{B}_{30}$, (d) $I2_12_12_1\text{-Na}_2\text{B}_{30}$, and (e) the experimental result at normal conditions.

Figure 4 shows band structures of $Imma\text{-Na}_2\text{B}_{30}$, $Imm2\text{-Na}_2\text{B}_{29}$, and $I2_12_12_1\text{-Na}_2\text{B}_{30}$ from the GGA-PBE calculations. Previously, $Imma\text{-Na}_2\text{B}_{30}$ was thought to be a metal [11]. However, our calculations show that valence and conduction bands exhibit linear dispersion at the Fermi level [Fig. 4(a)]. Further band analysis of $Imma\text{-Na}_2\text{B}_{30}$ indicates that the crossing points form two perpendicular nodal rings [Fig. 4(b)], which are dominantly originated from the p orbitals of B atoms. Therefore, $Imma\text{-Na}_2\text{B}_{30}$ is a topological nodal line semimetal. The particular nodal rings should be protected by the combination of inversion and time-reversal symmetry [27], which are expected to have more intensive nonlinear electromagnetic response than Dirac semimetals with a single cone and thus possess a higher efficiency of carrier transport at the Fermi level via multiple Dirac channels [28]. In $Imm2\text{-Na}_2\text{B}_{29}$, due to very close structure similarity, the nodal rings could be preserved. However, because of the minor concentration of B vacancies, the Fermi level is shifted down by 0.62 eV to the valence band [Fig. 4(c)], consequently the hybridized bonding states located at the valence band are partially filled, hence $Imm2\text{-Na}_2\text{B}_{29}$ is metallic. In contrast, $I2_12_12_1\text{-Na}_2\text{B}_{30}$ is an indirect-gap semiconductor with a band gap of 1.6 eV [Fig. 4(d)]. Therefore, as mentioned above, in view of the energetic stability, we see the order of stability $I2_12_12_1\text{-Na}_2\text{B}_{30} > Imma\text{-Na}_2\text{B}_{30} > Imm2\text{-Na}_2\text{B}_{29}$, which is in accordance with the electronic stability among the three compounds, that is, the semiconducting $I2_12_12_1\text{-Na}_2\text{B}_{30} >$ semimetallic $Imma\text{-Na}_2\text{B}_{30} >$ metallic $Imm2\text{-Na}_2\text{B}_{29}$.

Phonon densities of states (PDOS) of $I2_12_12_1\text{-Na}_2\text{B}_{30}$ and $Imma\text{-Na}_2\text{B}_{30}$ phases are shown in Fig. 5(a), both of them

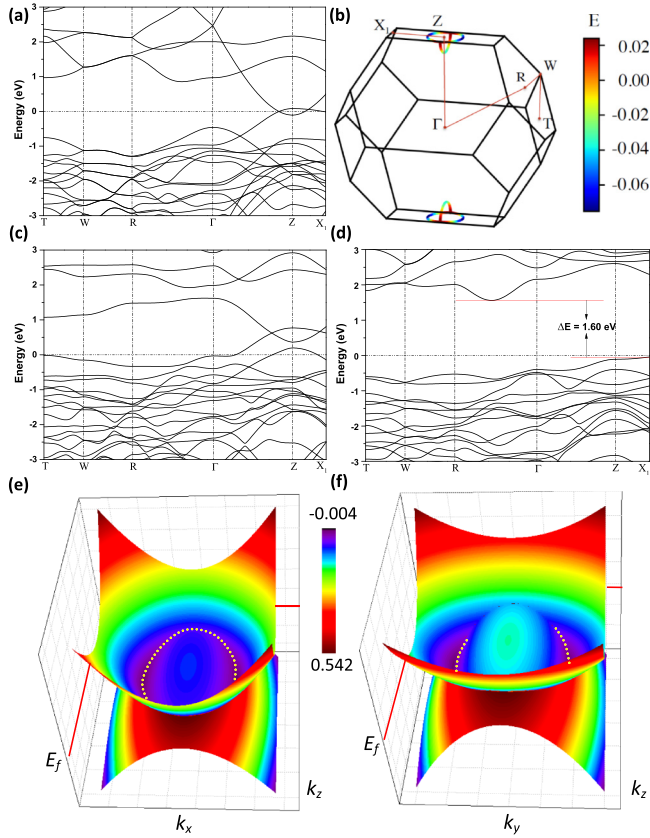


FIG. 4. (a) The band structure of $Imma\text{-Na}_2\text{B}_{30}$ at ambient pressure. (b) Several high-symmetry points in the Brillouin zone of $Imma\text{-Na}_2\text{B}_{30}$ are labeled. The multiple nodal rings center at the Z point, and the color bar indicates the energy of each nodal point. (c) and (d) show the band structures of $Imm2\text{-Na}_2\text{B}_{29}$ and $I2_12_12_1\text{-Na}_2\text{B}_{30}$ at ambient pressure. (e) and (f) show the band crossings (indicated by the yellow dotted lines) of $Imma\text{-Na}_2\text{B}_{30}$ formed by the valence and conduction bands in the vicinity of the Z point.

are dynamically stable at ambient pressure. In addition, the temperature dependence of the free energy of $I2_12_12_1\text{-Na}_2\text{B}_{30}$ and $Imma\text{-Na}_2\text{B}_{30}$ is shown in Fig. 5(b): $I2_12_12_1\text{-Na}_2\text{B}_{30}$ is always more stable than $Imma\text{-Na}_2\text{B}_{30}$ at least up to the temperature of 1000 K. We also calculated charge distributions of $Imma\text{-Na}_2\text{B}_{30}$ and $I2_12_12_1\text{-Na}_2\text{B}_{30}$. Bader charges show significant differences for the interstitial B atoms: In $Imma\text{-Na}_2\text{B}_{30}$, they are $+0.38$ and $-1.15e$ for B3 and B5 atoms, whereas they are $+0.03$ and $+0.07e$ for the interstitial B1 and B8 atoms of the $I2_12_12_1\text{-Na}_2\text{B}_{30}$ structure. More homogeneous Bader charges in the interstitial sublattice correlate with their greater thermodynamic stability at ambient pressure, in agreement with the proposed correlations between local bonding configurations and energetic stability [29,30]. Hence the free energy, electronic stability, formation energy, and charge transfer support that $I2_12_12_1\text{-Na}_2\text{B}_{30}$ is a true thermodynamic ground state, unlike $Imm2\text{-Na}_2\text{B}_{29}$ and $Imma\text{-Na}_2\text{B}_{30}$. Furthermore, boron-rich sodium borides are expected to have superior mechanical properties, e.g., high hardness. According to models [31,32], Vickers hardness was estimated as $H_v = 0.92k^{1.137}G^{0.708}$ and $k = G/B$, where G and B are the shear modulus and the bulk modulus. The

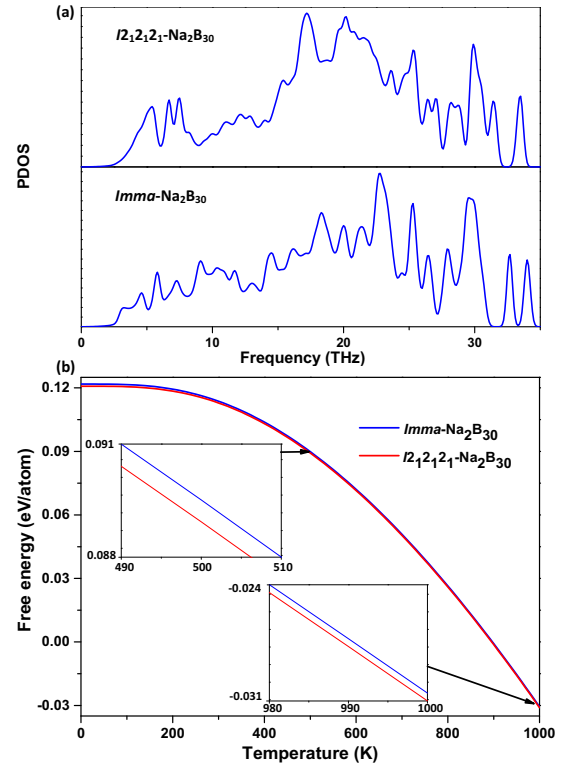


FIG. 5. (a) Phonon DOS of $I2_12_12_1\text{-Na}_2\text{B}_{30}$ and $Imma\text{-Na}_2\text{B}_{30}$ at ambient pressure. (b) The temperature dependence of the free energy for $I2_12_12_1\text{-Na}_2\text{B}_{30}$ and $Imma\text{-Na}_2\text{B}_{30}$ at ambient pressure. The insets show the free energies near 500 and 1000 K.

calculated hardnesses for $Imm2\text{-Na}_2\text{B}_{29}$, $Imma\text{-Na}_2\text{B}_{30}$, and $I2_12_12_1\text{-Na}_2\text{B}_{30}$ (see Table I) are 25.5, 30.2, and 37.4 GPa, respectively. Thus the semiconducting $I2_12_12_1\text{-Na}_2\text{B}_{30}$ phase is harder than semimetallic $Imma\text{-Na}_2\text{B}_{30}$ or metallic $Imm2\text{-Na}_2\text{B}_{29}$, owing to its special interstitial helical structure, which enhances the energetic stability and hardness.

In conclusion, we performed a systematic search for stable compounds of sodium and boron and identified semiconducting $I2_12_12_1\text{-Na}_2\text{B}_{30}$ as a new ground-state structure, which has an unprecedented three-dimensional boron framework with the peculiar interstitial helical structure. Recently, a new silicon allotrope with a quasidirect band gap was synthesized by using a novel two-step synthesis methodology [33] (consisting of the synthesis of $\text{Na}_4\text{Si}_{24}$ and then removing the Na atoms from the open-framework $\text{Na}_4\text{Si}_{24}$ structure by the thermal “degassing” process). Since the channel-like boron host structure is also present in $I2_12_12_1\text{-Na}_2\text{B}_{30}$ (along the b axis), one can attempt to synthesize a new boron allotrope ($I2_12_12_1\text{-B}_{30}$) by using the same approach.

This Rapid Communication was supported by the National Science Foundation of China (Grants No. 11674176 and No. 51772263), the Tianjin Science Foundation for Distinguished Young Scholars (Grant No. 17JJCJQC44400), and the 111 Project (Grant No. B07013). A.R.O. thanks Russian Science Foundation (Grant No. 17-73-20038), and the Foreign Talents Introduction and Academic Exchange Program (Grant No. B08040). Q.Z. is grateful for support from the National Nuclear

Security Administration under the Stewardship Science Academic Alliances Program through DOE Cooperative Agreement No. DE-NA0001982. X.D. acknowledges the computing

resources of Tianhe II and the support of Chinese National Supercomputer Center in Guangzhou. Q.S.W. acknowledges support by the NCCR MARVEL.

-
- [1] J. Nagamatsu, N. Nakagawa, T. Muranaka, Y. Zenitani, and J. Akimitsu, *Nature (London)* **410**, 63 (2001).
- [2] H. Y. Chung, M. B. Weinberger, J. B. Levine, R. W. Cumberland, A. Kavner, J. M. Yang, S. H. Tolbert, and R. B. Kaner, *Science* **316**, 436 (2007).
- [3] R. Mohammadi, A. T. Lech, M. Xie, B. E. Weaver, M. T. Yeung, S. H. Tolbert, and R. B. Kaner, *Proc. Natl. Acad. Sci. USA* **108**, 10958 (2011).
- [4] G. Akopov, M. T. Yeung, and R. B. Kaner, *Adv. Mater.* **29**, 1604506 (2017).
- [5] H. Jang, G. Friemel, J. Ollivier, A. V. Dukhnenko, N. Y. Shitsevalova, V. B. Filipov, B. Keimer, and D. S. Inosov, *Nat. Mater.* **13**, 682 (2014).
- [6] M. Neupane, N. Alidoust, S.-Y. Xu, T. Kondo, Y. Ishida, D. J. Kim, C. Liu, I. Belopolski, Y. J. Jo, T.-R. Chang, H.-T. Jeng, T. Durakiewicz, L. Balicas, H. Lin, A. Bansil, S. Shin, Z. Fisk, and M. Z. Hasan, *Nat. Commun.* **4**, 2991 (2013).
- [7] R. Naslain and J. S. Kasper, *J. Solid State Chem.* **1**, 150 (1970).
- [8] B. Albert, K. Hofmann, C. Fild, H. Eckert, M. Schleifer, and R. Grurhn, *Chem. Eur. J.* **6**, 2531 (2000).
- [9] B. Albert, *Angew. Chem., Int. Ed.* **37**, 1117 (1998).
- [10] B. Albert and H. Hillebrecht, *Angew. Chem., Int. Ed.* **48**, 8640 (2009).
- [11] <https://www.materialsproject.org/>.
- [12] A. R. Oganov and C. W. Glass, *J. Chem. Phys.* **124**, 244704 (2006).
- [13] W. Zhang, A. R. Oganov, A. F. Goncharov, Q. Zhu, S. E. Boulfelfel, A. O. Lyakhov, M. Somayazulu, and V. B. Prakapenka, *Science* **342**, 1502 (2013).
- [14] Q. Zhu, D. Y. Jung, A. R. Oganov, C. W. Glass, C. Gatti, and A. O. Lyakhov, *Nat. Chem.* **5**, 61 (2013).
- [15] Y. L. Li, S. N. Wang, A. R. Oganov, H. Gou, J. S. Smith, and T. A. Strobel, *Nat. Commun.* **6**, 6974 (2015).
- [16] X. Dong, A. R. Oganov, A. F. Goncharov, E. Stavrou, S. Lobanov, G. Saleh, G. R. Qian, Q. Zhu, C. Gatti, V. L. Deringer, R. Dronskowski, X. F. Zhou, V. B. Prakapenka, Z. Konôpková, I. A. Popov, A. I. Boldyrev, and H. T. Wang, *Nat. Chem.* **9**, 440 (2017).
- [17] P. E. Blöchl, *Phys. Rev. B* **50**, 17953 (1994).
- [18] G. Kresse and J. Furthmüller, *Phys. Rev. B* **54**, 11169 (1996).
- [19] J. P. Perdew, K. Burke, and M. Ernzerhof, *Phys. Rev. Lett.* **77**, 3865 (1996).
- [20] D. M. Ceperley and B. J. Alder, *Phys. Rev. Lett.* **45**, 566 (1980).
- [21] J. P. Perdew and A. Zunger, *Phys. Rev. B* **23**, 5048 (1981).
- [22] A. Togo, F. Oba, and I. Tanaka, *Phys. Rev. B* **78**, 134106 (2008).
- [23] R. Hill, *Proc. Phys. Soc. A* **65**, 349 (1952).
- [24] S. J. Clark, M. D. Segall, C. J. Pickard, P. J. Hasnip, M. I. J. Probert, K. Refson, and M. C. Payne, *Z. Kristallogr.* **220**, 567 (2005); <http://accelrys.com/products/collaborative-science/biovia-materials-studio/>.
- [25] A. A. Mostofi, J. R. Yates, Y.-S. Lee, I. Souza, D. Vanderbilt, and N. Marzari, *Comput. Phys. Commun.* **178**, 685 (2008).
- [26] Q. S. Wu, S. N. Zhang, H.-F. Song, M. Troyera, and A. A. Soluyanov, *Comput. Phys. Commun.* **224**, 405 (2018).
- [27] Q. Xu, R. Yu, Z. Fang, X. Dai, and H. M. Weng, *Phys. Rev. B* **95**, 045136 (2017).
- [28] Y. Jiao, F. Ma, C. Zhang, J. Bell, S. Sanvito, and A. Du, *Phys. Rev. Lett.* **119**, 016403 (2017).
- [29] X.-F. Zhou, Q.-R. Qian, J. Zhou, B. Xu, Y. Tian, and H.-T. Wang, *Phys. Rev. B* **79**, 212102 (2009).
- [30] X.-F. Zhou, A. R. Oganov, G.-R. Qian, and Q. Zhu, *Phys. Rev. Lett.* **109**, 245503 (2012).
- [31] Y. Tian, B. Xu, and Z. Zhao, *Int. J. Refract. Met. Hard Mater.* **33**, 93 (2012).
- [32] X. Q. Chen, H. Niu, D. Li, and Y. Li, *Intermetallics* **19**, 1275 (2011).
- [33] D. Y. Kim, S. Stefanoski, O. O. Kurakevych, and T. A. Strobel, *Nat. Mater.* **14**, 169 (2015).